Non-Abelian SU(2) gauge fields through density wave order and strain in graphene

Sarang Gopalakrishnan, Pouyan Ghaemi, and Shinsei Ryu

Phys. Rev. B **86**, 081403 — Published 13 August 2012

DOI: 10.1103/PhysRevB.86.081403

Non-Abelian $SU(2)$ gauge fields through density-wave order and strain in graphene

Sarang Gopalakrishnan, Pouyan Ghaemi, and Shinsei Ryu
Department of Physics, University of Illinois at Urbana-Champaign, 1110 West Green Street, Urbana, Illinois 61801
(Dated: May 12, 2012)

Spatially varying strain patterns can qualitatively alter the electronic properties of graphene, acting as effective valley-dependent magnetic fields and giving rise to pseudo-Landau-level (PLL) quantization. Here, we show that the strain-induced magnetic field is one component of a non-Abelian $SU(2)$ gauge field within the low-energy theory of graphene, and identify the other two components as period-3 charge-density waves. We show that these density-waves, if spatially varied, give rise to PLL quantization. We also argue that strain-induced magnetic fields can induce density-wave order in graphene, thus dynamically gapping out the lowest PLL; moreover, the ordering should generically be accompanied by dislocations. We discuss experimental signatures of these effects.

The discovery of graphene[1]—a carbon monolayer with low-energy electronic properties governed by the Dirac equation[2]—has stimulated enormous interest in condensed matter systems having Dirac quasiparticles. Although other systems supporting Dirac quasiparticles have subsequently been discovered (e.g., the surface bands of topological insulators[3,4]), graphene is uniquely tunable through lattice deformations and strains, being a soft two-dimensional membrane[2]. Strain alters the electronic structure of graphene by modulating the hopping amplitudes between neighboring lattice sites. A striking example of the electronic consequences of strain is that certain spatially varying strain patterns can mimic the effects of a pseudo-"magnetic field" that has opposite signs in the vicinity of the two Dirac points (which we shall refer to as the valleys $\mathbf{K}$ and $\mathbf{K}'$[5]). Such pseudo-magnetic fields, on the order of 300 Tesla, were recently demonstrated in pioneering experiments[6] on nanoscale graphene bubbles; subsequently, effective fields greater than 60 Tesla were also realized in "molecular graphene"[7]. At these fields, each valley is deep in the quantum Hall regime, so that its electronic structure consists of well-spaced pseudo-Landau levels (PLLs). Because the PLLs are highly degenerate, one expects correlation effects to be strong within them; indeed, recent works have shown that, in the presence of interactions, partially-filled PLLs are unstable to forming ordered states such as valley ferromagnets, spin-Hall phases and triplet superconductors[8,9].

In the present work we show that the strain-induced, valley-dependent magnetic field is one component of a non-Abelian $SU(2)$ gauge field within the low-energy theory of graphene. We identify the other two generators of this $SU(2)$ gauge field as period-3 charge-density waves (3CDWs) (Fig. 1) that mix the $\mathbf{K}$ and $\mathbf{K}'$ valleys. We show that these charge-density waves act as gauge potentials: when their amplitude is constant, they move the Dirac cones [Fig. 2(B)]; but when their amplitude is spatially varied, they give rise to Landau-level quantization, as shown in Fig. 3. Although methods for realizing non-Abelian $SU(2)$ gauge fields had previously been proposed in ultracold atomic settings[10–12], twisted bilayer graphene[13], and fullerene molecules[14], such fields have yet to be experimentally realized in condensed matter. The present work suggests an alternative approach, which might be easier to implement, e.g., in molecular graphene[7].

Having established the $SU(2)$ gauge structure, we turn to the effects of the 3CDW patterns on the strain-induced PLL structure. We find that, although these perturbations do not open up gaps in unstrained graphene, they *do* gap out the lowest (i.e., zero-energy) PLL. On general grounds, then, we expect these gaps, and the corresponding 3CDW patterns, to be dynamically generated by electron-electron or electron-phonon interactions whenever graphene is strained, as they would reduce the ground-state energy. (The relation between different mass gaps and the corresponding ordered states was previously explored, for unstrained graphene, in Refs.[15–18].)

After discussing the 3CDW patterns, we turn to their defects (i.e., dislocations), and show that these defects are entwined with the ordering in a distinctive way, owing to the valley-dependence of the pseudo-magnetic field. In contrast with the case of a regular field, for a strain-induced field a uniform 3CDW perturbation does *not* mix the spatially coincident Landau orbitals in the two valleys, as these are *counter-propagating*. However, a 3CDW perturbation with a defect at the origin can mix the valleys and open up a gap. Thus, in experimental geometries such as that of Ref.[6], the defects as well as the order are likely to be dynamically generated.

Model. In the absence of interactions, the tight-binding Hamiltonian of strained graphene reads as

$$H_0 = \sum_{\mathbf{r}_i} \sum_{a=1,2,3} (t + \delta t_a(\mathbf{r}_i))(a^\dagger(\mathbf{r}_i) b(\mathbf{r}_i + \boldsymbol{\delta}_a) + h.c.), \quad (1)$$

where $\delta t_a(\mathbf{r}_i)$ is the strain-induced variation of the nearest neighbour hopping amplitude between the A-sublattice site at $\mathbf{r}_i$ and the B-sublattice site at $\mathbf{r}_i + \boldsymbol{\delta}_a$ of the honeycomb lattice[2]. The vectors $\boldsymbol{\delta}_a$ connect any A-sublattice atom to its three B-sublattice nearest neighbors. In the absence of strain, the low-energy excitations correspond to linearly dispersing states close to the two Dirac points at momenta $\pm\mathbf{K}$ with $\mathbf{K} = (4\pi/3\sqrt{3}a_0)\mathbf{e}_\mathbf{x}$, a_0 being the carbon-carbon bond length[2]. Near the Dirac points $\mathbf{K}$ and $\mathbf{K}'$ the wavefunctions of such states can be written as four-component spinors

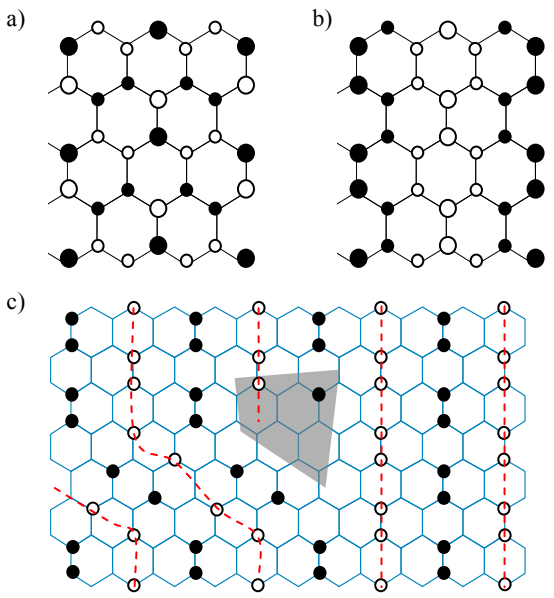

FIG. 1. $SU(2)$ gauge potentials [i.e., charge-density-wave (3CDW) patterns] and their defects. Panels (a) and (b) show the patterns corresponding to $\zeta_{x,1}$ and $\zeta_{y,2}$ respectively (see Table I); the remaining patterns are related to these by translation. Black (white) circles denote excess positive (negative) charge; larger circles correspond to greater excess charge. Panel (c) sketches a dislocation in the 3CDW pattern; the dislocation core is marked in gray. Dashed red lines trace crests of the 3CDW pattern.

$\Psi \equiv (\psi_{A,\mathbf{K}}, \psi_{B,\mathbf{K}}, \psi_{A,\mathbf{K}'}, \psi_{B,\mathbf{K}'})$ where the first index denotes the component of the wavefunction on the $A(B)$ sublattice of the honeycomb unit cell, and the second index denotes the component of the state that is associated with the $\mathbf{K}$ ($\mathbf{K}'$) valley. The low energy effective Hamiltonian close to the Dirac points reads as:

$$\mathcal{H}_0 = v_F \left[\hat{p}_x \Gamma_x + \hat{p}_y \Gamma_y\right] \tag{2}$$

where $\Gamma_x = \tau_3\sigma_1$, $\Gamma_y = \tau_0\sigma_2$, v_F is the Fermi velocity, and the σ and τ operators are Pauli matrices acting on sublattice and valley indices respectively. We have not included the physical spin index as it does not affect our analysis, provided that the spin-orbit coupling is negligible.

There are three terms in the low-energy theory (i.e., "charges") that commute with the Hamiltonian (2): $Q_1 \equiv -\tau_2\sigma_2$, $Q_2 \equiv \tau_1\sigma_2$, $Q_3 \equiv \tau_3\sigma_0$. These realize an $SU(2)$ pseudo-spin algebra $[Q_i, Q_j] = 2i\epsilon_{ijk}Q_j$. We also define the electromagnetic $U(1)$ charge $Q_0 \equiv \tau_0\sigma_0$ (i.e., the identity operator), which commutes with the other charges. We can minimally couple $\mathcal{H}_0$ to the gauge potentials associated with these charges, arriving at the Hamiltonian:

$$\mathcal{H} = v_F \left[\Gamma_x \left(\hat{p}_x - \sum_{i=0}^{3} A_x^i Q_i\right) + \Gamma_y \left(\hat{p}_y - \sum_{i=0}^{3} A_y^i Q_i\right)\right]. \tag{3}$$

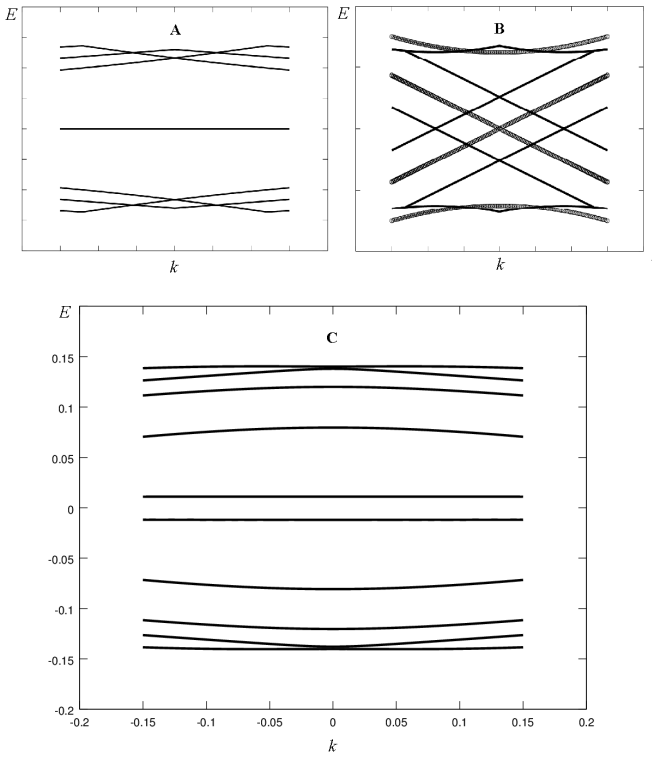

FIG. 2. (A) Band structure in the presence of strain, calculated for a 100-site thick graphene nanoribbon with zigzag edges, showing pseudo-Landau levels (PLLs). All energies are computed in terms of the unperturbed hopping; in the presence of strain, the hopping along one of the three directions increases linearly from t to $1.9t$ across the sample. The zero-energy level is in fact fourfold degenerate, including two zero-energy PLLs and two modes localized on zigzag edges. (B) Location of Dirac cones in the absence of strain, both with the perturbation $\zeta_{x,i}$ (thin solid line) and without it (thick line). Constant gauge potentials (see main text) are expected to shift the Dirac cones. (C) Band structure in the presence of both strain and $\zeta_{x,i}$. The fourfold-degenerate zero-energy mode is split; the two more widely separated levels correspond to the lowest PLL. (This was checked by computing the wavefunctions.)

We turn to the microscopic origins of the $SU(2)$ gauge potentials, $\zeta_{\mu,i} \equiv \Gamma_\mu Q_i$, where $\mu = x, y$ and $i = 1, 2, 3$. Of these, $\zeta_{\mu,3}$ comprise the familiar strain-induced vector potential. Strain generates a gauge field given by $A_x^0 + iA_y^3 = \sum_{a=1,2,3} \delta t_a(\mathbf{r}) e^{\pm i\mathbf{K}\cdot\boldsymbol{\delta}_a}$ near the Dirac points $\pm\mathbf{K}$. Note that $\sum_{a=1,2,3} \delta t_a(\mathbf{r}) e^{\pm i\mathbf{K}\cdot\boldsymbol{\delta}_a}$ is complex because the nearest-neighbor hoppings are not symmetric under inversion. The real part of the strain gauge field A_x^0 is the same in both valleys and therefore couples to Q_0; it can be gauged away assuming time-reversal symmetry holds. On the other hand, the imaginary part iA_y^3 has opposite sign in the two valleys and couples to Q_3, leading to the valley-dependent magnetic fields realized in the experiments of Refs.[6,7].

The four remaining gauge potentials (see Table I) orig-

Term	Low-energy	LPLL	Microscopic
$\zeta_{x,1}$	$\tau_1\sigma_3$	τ_1	$\cos(\mathbf{G}\cdot\mathbf{r})\cos\left[\pi(y/a_0+\frac{1}{4})\right]$
$\zeta_{x,2}$	$\tau_2\sigma_3$	τ_2	$\sin(\mathbf{G}\cdot\mathbf{r})\cos\left[\pi(y/a_0+\frac{1}{4})\right]$
$\zeta_{y,1}$	$\tau_2\sigma_0$	τ_2	$\sin(\mathbf{G}\cdot\mathbf{r})$
$\zeta_{y,2}$	$\tau_1\sigma_0$	τ_1	$\cos(\mathbf{G}\cdot\mathbf{r})$

TABLE I. Density-wave-based gauge potentials. This table lists microscopic and low-energy forms of the potentials, as well as forms when projected onto the lowest pseudo-Landau level (LPLL).

inate, as we shall now see, as 3CDWs. That they should be charge density waves can be seen as follows: (a) the perturbations mix the valleys, and must therefore involve spatial modulations that enlarge the unit cell[19]; (b) they do not mix the sublattices (i.e., they are proportional either to σ_3 or to σ_0), and can therefore include only on-site charge offsets and intra-sublattice (e.g., next-nearest neighbor) hopping. Two simple perturbations satisfying both criteria are charge modulations of wavevector $\mathbf{G}$ (where $\mathbf{G}\equiv\mathbf{K}-\mathbf{K}'$ is a vector connecting the two Dirac points), which realize τ_1 and τ_2 respectively:

$$\tau_1 \leftrightarrow \cos(\mathbf{G}\cdot\mathbf{r}), \quad \tau_2 \leftrightarrow \sin(\mathbf{G}\cdot\mathbf{r}). \tag{4}$$

The gauge potentials $\zeta_{x,i}$ are realized when the density waves on A and B sublattices are π out of phase, whereas the potentials $\zeta_{y,i}$ are realized when the density waves on the A and B sublattices are in phase. Fig. 1 shows the two corresponding density-wave arrangements, which are listed in Table I.

Numerical band structure calculations on nano-ribbons including these terms are shown in Figs. 2 and 3; evidently, the ζ's do not open up gaps in the absence of strain, but shift the Dirac points in momentum space, as a vector potential is expected to do. Moreover, if the coefficient of $\zeta_{y,2}$, say, is varied linearly with x (cf. the Landau gauge description of a uniform magnetic field), it gives rise to PLL quantization as shown in Fig. 3. Hence these terms can be regarded, together with the strain-induced gauge potentials, as enabling the realization of a general $SU(2)$ gauge field.

Strain-induced PLLs and their mass gaps. The pseudospin $SU(2)$ symmetry (at low energies) allowed us to treat the strain and 3CDWs on the same footing above. We now break this symmetry by considering the PLL structure created by a strain pattern inducing a uniform pseudo-magnetic field. The eigenstates of $\mathcal{H}$ then fall into PLLs at energies $E_n \sim \sqrt{n}$, and in particular there is a PLL at zero energy in each valley[2], which we term the LPLL. While the LPLL shares some features with the zero-energy Landau levels induced by a real magnetic field, it is distinct in two essential ways, as follows. (1) In contrast with the case of a real magnetic field (in which the lowest Landau level wavefunctions in the two valleys are located on opposite sublattices), the LPLL wavefunctions in both valleys are located entirely on the A sublattice[8]. (2) The LPLL wavefunctions in the $\mathbf{K}(\mathbf{K}')$ valleys have the four-component form $\Psi^{\mathbf{K}}_{0,m} = (\phi_{0,m},0,0,0)$ and $\Psi^{\mathbf{K}'}_{0,m} = (0,0,\phi^*_{0,m},0)$, respectively, where $\phi_{0,m}$ is the mth Landau orbital in the lowest (nonrelativistic) Landau level (see below). [By contrast, for a *real* magnetic field, the second of these would be $\Psi^{\mathbf{K}'}_{0,m} = (0,0,0,\phi_{0,m})$.] Thus, in a pseudo-magnetic field, the PLL orbitals are *counter-propagating*, whereas in a real magnetic field they are *co-propagating*. For a *real* magnetic field, the valley index can therefore be regarded as a mere flavor degree of freedom, and a uniform valley-mixing perturbation mixes Landau orbitals in the two valleys. However, for *strained* graphene, the valley index should not be interpreted as a flavor index, because the wavefunctions in the two valleys are spatially distinct. As argued below, this implies that mass terms with *defects* are necessary to gap the LPLL. The precise consequences depend on *which gauge* in pseudo-vector potentials is simulated by the strain. (This is possible because, while two gauge-equivalent electromagnetic vector potentials are physically identical, different pseudo-vector potentials correspond to different strain patterns and are thus *microscopically* distinct; therefore, the physics of pseudo-magnetic fields is not guaranteed to be gauge-invariant.)

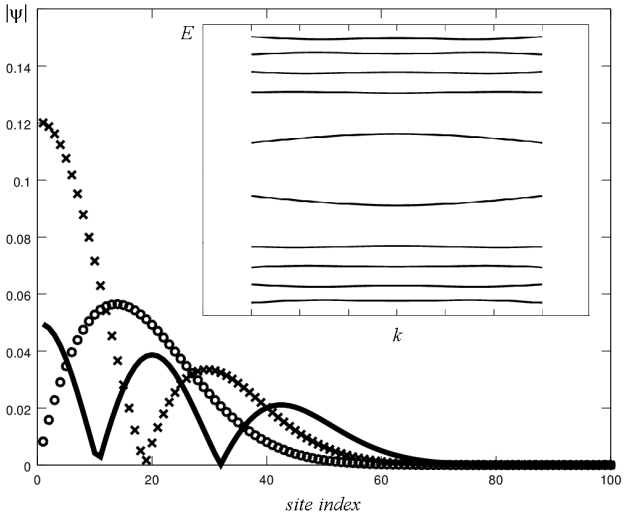

FIG. 3. Pseudo-Landau levels (PLLs) generated by the $SU(2)$ pseudo-gauge potential $A_x^2 Q_2 = BQ_2 y$ on a 100-site nanoribbon with zigzag edges. Potential strength varies linearly from zero at one end of the ribbon to $0.74t$ at the other end. Main panel shows wavefunctions in the lowest three distinct PLLs, calculated on a 100-site nanoribbon with zigzag edges. Inset shows the PLL structure (cf. Fig. 2A), indicating that the PLLs are indeed flat for momenta near the Dirac points.

Uniform perturbations. We now address point (1) above, ignoring spatial structure and considering the effects of uniform (i.e., defect-free) 3CDW perturbations precisely *at* the Dirac point. Many of the properties of the LPLL follow from its trivial sublattice structure: in particular, one can find the form of any perturbation in

the LPLL by projecting it onto the A sublattice. Thus, perturbations within the LPLL are completely described by 2×2 matrices in τ (i.e., valley) space (Table I); and several perturbations that open up gaps in *unstrained* graphene, such as an intra-unit-cell charge-density wave ($\sigma_3\tau_0$) and the Kekulé distortion ($\sigma_1\tau_1$), are trivial when projected to the LPLL. However, the $SU(2)$ gauge potentials $\zeta_{\mu,i}$ *do* gap out the LPLL, as they project onto either τ_1 or τ_2 (Table I), and can thus mix LPLL orbitals from the $\mathbf{K}$ and $\mathbf{K}'$ valleys.

Two further perturbations that split the LPLL are valley polarization, $m_p \equiv \tau_3\sigma_0$, and the Haldane mass[20], $m_H \equiv \tau_3\sigma_3$. Within the LPLL, these terms are *equivalent*; both correspond to τ_3, which shifts the energy of one valley relative to the other. Both terms anticommute with the gauge fields; therefore, within the low-energy theory, it seems that these gaps can be continuously deformed into one another. (Thus, the fate of the topologically-protected edge mode associated with m_H cannot be addressed within the low-energy theory. Numerical calculations of the band structure in the presence of both m_H and $\zeta_{x,i}$ suggest that as $\zeta_{x,i}$ is increased, the edge state drifts away from the Dirac points; it is therefore plausible that $\zeta_{x,i}$ and m_H compete away from the Dirac points. We shall revisit this question in future work.)

The perturbations discussed above are likely to be dynamically generated in experiments with neutral graphene (i.e., a half-filled LPLL), as opening up a gap would lower the ground-state energy. The 3CDWs could arise either because of electron-phonon or electron-electron interactions; moreover, electron-electron interactions can give rise to a spontaneous valley polarization[8].

Momentum dependence. We now turn to the second distinctive feature of the PLLs [point (2) above] and discuss the role played by the spatial structure of PLL wavefunctions. To address this, we shall consider the nature of the 3CDW perturbations on orbitals *away* from the Dirac point.

We first consider the strain pattern realizing the Landau gauge; here, if the 3CDW amplitude is uniform, the $\mathbf{K}$-valley Landau orbital $\phi_{0,m}(x,y) \propto e^{i\frac{2\pi m}{L}x}e^{-\left(y-\frac{2\pi m}{L}l^2\right)^2/l^2}$ (l being the magnetic length) can hybridize *only* with the $\mathbf{K}'$-valley orbital $\phi^*_{0,-m}(x,y) \propto e^{i\frac{2\pi m}{L}x}e^{-\left(y+\frac{2\pi m}{L}l^2\right)^2/l^2}$, due to the conservation of k_x. The overlap between these two states, though nonzero, *decreases* as $|m|$ is increased, and becomes exponentially small for $ml \gg L$. This decrease of overlap leads to the convexity of the LPLL gap (Fig. 2), and implies that the 3CDW gap is an inherently mesoscopic phenomenon. (However, note that all experimental realizations of pseudo-magnetic fields in strained graphene involve mesoscopic systems.)

Point defects. If the strain realizes a symmetric gauge pattern, $\phi_{0,m}(r,\theta) \propto e^{im\theta}r^m e^{-r^2/l^2}$, as in the experiments of Ref.[6], the consequences are even more striking. Here, the only allowed orbitals have $m \geq 0$; otherwise $\phi_{0,m}$ is not normalizable. As a result, *no* uniform perturbation can gap out the $m \neq 0$ orbitals. Thus, in order to open up a gap, it is necessary to consider perturbations having defects, i.e., edge dislocations in the 3CDW case. Within the LPLL, the two independent 3CDW orders are represented by τ_1 and τ_2 (Table I). The 3CDWs can support edge dislocations [Fig. 1(c)], which appear as vortices within the LPLL theory:

$$\Delta(r)\left[\tau_1\cos(n\theta)+\tau_2\sin(n\theta)\right] = \begin{pmatrix} 0 & \Delta(r)e^{in\theta} \\ \Delta(r)e^{-in\theta} & 0 \end{pmatrix} \tag{5}$$

where $\Delta(r)$ is a function that vanishes at $r=0$ and is constant for $r \gg l_M$. Such vortex solutions carry angular momentum, and can thus hybridize LPLL orbitals: for vorticity n, any orbital with $m < n$ can hybridize with the orbital with $m' = n-m$. Hence a larger vorticity can gap out more Landau orbitals, leading to lower energy (although it might also cost greater electrostatic or elastic energy). Therefore, one expects defects to be dynamically generated along with the 3CDW patterns.

Effects in higher PLLs. We now turn to the effects of the aforementioned perturbations within the higher PLLs. Here, the sublattice structure is not trivial, so that the six masses are *distinct* perturbations. These perturbations fall into two classes, depending on whether their sublattice component is σ_0 or σ_3. Perturbations of the former class split all the PLLs. For m_p, this is clear by inspection; similarly, one can see from degenerate perturbation theory that $\zeta_{y,i}$ mix $\Psi^{\mathbf{K}}_{n,m}$ and $\Psi^{\mathbf{K}'}_{n,m}$ (assuming the strain pattern realizes the Landau gauge). However, m_H and $\zeta_{x,i}$ do *not* mix $\Psi^{\mathbf{K}}_{n,m}$ and $\Psi^{\mathbf{K}'}_{n,m}$, and thus preserve the double degeneracy of higher PLLs. However, these perturbations *do* mix $\Psi^{\mathbf{K}}_{n,m}$ and $\Psi^{\mathbf{K}'}_{-n,m}$, thus shifting the energy of the nth PLL by $\alpha^2/(2\Delta_0\sqrt{n})$, where Δ_0 is the cyclotron energy scale.

These considerations might influence which perturbations are dynamically generated in experiments. If one of the nonzero PLLs is half-filled, the favored perturbations are of the σ_0 class; by contrast, at half-filling of the LPLL (i.e., for neutral graphene), the σ_3 perturbations are preferred, as these lower the energy of the filled negative-energy PLLs. Moreover, because the perturbations with τ_3 open up momentum-independent gaps, they are preferred at the level of the low-energy theory; thus, in agreement with Ref.[21], a low-energy analysis would predict that the Haldane mass is likeliest to be generated in the case of a half-filled LPLL. However, it should be emphasized that these considerations can generically be outweighed by changes in the band structure away from the Dirac points.

Experimental aspects. We close by touching upon some experimental considerations. The 3CDW ordering described here can either be dynamically generated via strain, or externally imposed. In the former case, the ordering can be readily detected via scanning-tunneling microscopy (STM); this technique is commonly used to study stripe ordering (see, e.g., Ref.[22]). Alternatively,

the 3CDW perturbations can be studied by *externally imposing* them. This is easiest to do for engineered systems, such as molecular graphene[7], where a 3CDW pattern such as $\zeta_{y,i}$ can be imposed by hand on the triangular network of adsorbate molecules (or, alternatively, for hexagonal optical lattices[23]). However, it might also be possible to realize it using systems of graphene grown on anisotropic substrates, which favor 3CDW formation.

Acknowledgments. S.G. and P.G. are indebted to Paul Goldbart for helpful discussions. The authors acknowledge support from DOE DE-FG02-07ER46453 (S.G.) and ICMT at UIUC (P.G.).

[1] K. S. Novoselov, A. K. Geim, S. V. Morozov, D. Jiang, M. I. Katsnelson, I. V. Grigorieva, S. V. Dubonos, and A. A. Firsov, Nature, **438**, 197 (2005).

[2] A. H. Castro Neto, F. Guinea, N. M. R. Peres, K. S. Novoselov, and A. K. Geim, Rev. Mod. Phys., **81**, 109 (2009).

[3] X.-L. Qi and S.-C. Zhang, Rev. Mod. Phys., **83**, 1057 (2011).

[4] M. Z. Hasan and C. L. Kane, Rev. Mod. Phys., **82**, 3045 (2010).

[5] F. Guinea, M. Katsnelson, and A. Geim, Nat. Phys., **6**, 30 (2010).

[6] N. Levy, S. A. Burke, K. L. Meaker, M. Panlasigui, A. Zettl, F. Guinea, A. H. Castro Neto, and M. F. Crommie, Science, **329**, 544 (2010).

[7] K. K. Gomes, W. Mar, W. Ko, F. Guinea, and H. C. Manoharan, Nature, **483**, 306 (2012).

[8] P. Ghaemi *et al.*, arXiv:1111.3640.

[9] D. Pesin and D. Abanin, arXiv:1112.6420.

[10] K. Osterloh, M. Baig, L. Santos, P. Zoller, and M. Lewenstein, Phys. Rev. Lett., **95**, 010403 (2005).

[11] Y.-J. Lin, K. Jiménez-García, and I. Spielman, Nature, **471**, 83 (2011).

[12] N. Goldman, A. Kubasiak, P. Gaspard, and M. Lewenstein, Phys. Rev. A, **79**, 023624 (2009).

[13] P. San-Jose, J. González, and F. Guinea, ArXiv:1110.2883 (2011).

[14] J. González, F. Guinea, and M. A. H. Vozmediano, Phys. Rev. Lett., **69**, 172 (1992).

[15] P. Ghaemi, S. Ryu, and D.-H. Lee, Phys. Rev. B, **81**, 081403 (2010).

[16] P. Ghaemi and S. Ryu, Phys. Rev. B, **85**, 075111 (2012).

[17] S. Ryu, C. Mudry, C.-Y. Hou, and C. Chamon, Phys. Rev. B, **80**, 205319 (2009).

[18] I. F. Herbut, Phys. Rev. B, **76**, 085432 (2007).

[19] C. Chamon, Phys. Rev. B, **62**, 2806 (2000).

[20] F. D. M. Haldane, Phys. Rev. Lett., **61**, 2015 (1988).

[21] I. F. Herbut, Phys. Rev. B, **78**, 205433 (2008).

[22] C. Howald, H. Eisaki, N. Kaneko, and A. Kapitulnik, Proc. Nat. Acad. Sci, **100**, 9705 (2003).

[23] P. Soltan-Panahi, J. Struck, P. Hauke, A. Bick, W. Plenkers, G. Meineke, C. Becker, P. Windpassinger, M. Lewenstein, and K. Sengstock, Nat. Phys., **7**, 434 (2011).